Oscillatory damping in long-time evolution of the surface quasi-geostrophic equations with generalised viscosity: a numerical study

Koji Ohkitani

Department of Applied Mathematics
School of Mathematics and Statistics
The University of Sheffield
Hicks Building, Hounsfield Road Sheffield S3 7RH, U.K.

E-mail: K.Ohkitani@sheffield.ac.uk

Takashi Sakajo

Department of Mathematics, Hokkaido University
Kita 10 Nishi 8 Kita-Ku Sapporo Hokkaido 060-0810, Japan
and
Precursory Research Embryonic Science Technology,
Japan Science and Technolgoy Agency,
3-5 Sanbancho, Chiyoda-ku, Tokyo 102-0075 Japan

E-mail: sakajo@math.sci.hokudai.ac.jp

Abstract.

We study numerically the long-time evolution of the surface quasi-geostrophic equation with generalised viscosity of the form $(-\triangle)^\alpha$, where global regularity has been proved mathematically for the subcritical parameter range $\alpha \geq 1/2$. Even in the supercritical range, we have found numerically that smooth evolution persists, but with a very slow and oscillatory damping in the long run. A subtle balance between nonlinear and dissipative terms is observed therein. Notably, qualitative behaviours of the analytic properties of the solution do not change in the super and subcritical ranges, suggesting the current theoretical boundary $\alpha = 1/2$ is of technical nature.

1. Introduction

The regularity issues on partial differential equations are challenging and important problems in mathematical fluid mechanics. In particular, the regularity of the 3D Navier-Stokes equations remains the well-known open problem. The case of 2D Euler equations is an exceptional case, where global existence results have been proved by the conservation of the vorticity. Even in two-dimensional fluid dynamical systems, the vorticity is not generally conserved, say, in the 2D Boussinesq equations or in the 2D

magnetohydrodynamic equations. In thse cases proving global regularity for ideal fluids is virtually impossible.

In this paper, we consider so-called surface quasi-geostrophic (SQG) equation which has attracted much attention recently. This equation is important not only as a test bed for 3D problems, but also as a geophysical application on its own.

The mathematical study of the 2D SQG equation was initiated by [9, 10]. Since then it has been investigated mathematically [5, 7, 8, 11, 17, 22, 24, 27] and numerically [3, 12, 21, 23] by many authors. Recent mathematical works employ the method of a generalised viscosity of the form $(-\Delta)^\alpha$ and attempt proving regularity with the exponent α as small as possible. The best mathematical result at the moment says that if $\alpha \geq 1/2$ we have global regularity for the case of infinite plane $\mathbb{R}^2$ [4, 19]. At the moment, it seems to be difficult to extend similar analyses for $\alpha < 1/2$.

From the numerical experiments undertaken so far, we may gather the following rough scenario. For $\nu = 0$, layers with steep gradient of the temperature (the active scalar) will form. We may get closer to this first (near-)singularity with increasing spatial resolutions. For slightly viscous case, one can avoid the singularity formation and the flow pattern will be changed drastically. In the end we expect that the flow is on its way to converge towards the trivial zero solution. But apparently this final stage of decay has not been discussed in detail in previous works. On the other hand, for a successful proof of regularity, the dynamics in the late evolution should be dominated by the linear dissipative term.

On the basis of computational results we may expect global regularity for slightly dissipative cases and even for the ideal cases. But it has turned out to be very hard to prove it. A couple of questions naturally arise here: i) Why is it so difficult ?, ii) Is $\alpha = 1/2$ a genuine boundary or of technical nature ?, and iii) How does the solution actually behave in the long run ?

To address these issues, we study the hypoviscous SQG equation numerically in this paper, in a attempt to shed some light upon the difficulty that analytical approaches are facing. In particular, we will be interested in the analytic property of the flow in the long term evolution.

We have carried out numerical simulations for an unprecedentedly long time to understand what is happening in the 'final' stage of evolution, by changing the parameter α around the critical value ($\alpha = 1/2$). The rest of this paper is organised as follows. In Section 2, mathematical formulation is given together with a recapitulation of previous works. In Section 3, numerical results are presented, including detailed analyses of the late stage evolution. Finally, Section 4 is devoted to summary and discussion.

2. Mathematical formulation and strategy

2.1. SQG equation

The surface quasi-geostrophic equation for an active scalar (temperature) $\theta(t, \boldsymbol{x})$ with generalised viscosity reads

$$\begin{aligned} \frac{\partial \theta}{\partial t} + (\boldsymbol{u} \cdot \nabla)\theta = & -\nu(-\Delta)^{\alpha}\theta, \\ \theta(0, \boldsymbol{x}) \qquad & = \theta_0(\boldsymbol{x}), \end{aligned}$$

where $\theta_0(\boldsymbol{x})$ is the initial condition and $0 \leq \alpha \leq 1$. The velocity is given by

$$\boldsymbol{u} = \nabla^{\perp}(-\Delta)^{-1/2}\theta,$$

or $\boldsymbol{u} = -\boldsymbol{R}^{\perp}[\theta]$. Here $\boldsymbol{R}^{\perp}$ is the skewed version of a Riesz operator $\boldsymbol{R} = -\nabla(-\triangle)^{-1/2}$ and $\nabla^{\perp} = (\partial_y, -\partial_x)$. Periodic boundary condition with period 2π is imposed both in the x and y directions.

Note that for $\alpha = 0$, the equation has a drag term. By a set of transformations, e.g. [2], $\theta = e^{-\nu t}\tilde{\theta}$, $\tilde{t} = \frac{1-e^{-\nu t}}{\nu}$ we may reduce it to the equation for an ideal fluid.

The SQG equation has originally been derived in the context of geophysical fluid dynamics. On the other hand, this equation has been studied as a test bed for a singularity formation in incompressible flows since the pioneering works of [9, 10]. A singularity suggested therein was shown to have an alternative interpretation in [23]. Later this double-exponential growth has had added support [3, 12], whereas a mathematical proof for global regularity is yet to be obtained.

2.2. Test problem

In this paper we will make a full use of the analyticity strip method[26] to keep track of the long time evolution of the SQG equation in detail, particularly in connection with the blow-up issue. Before doing that, it makes sense to convince ourselves that such a numerical methodology actually works for such a delicate problem of inviscid singularity.

Take, for example, the 1D Burgers equation with hypoviscosity ($0 \leq \alpha \leq 1$):

$$u_t + uu_x = -\nu(-\partial_{xx})^{\alpha}u,$$

with the initial data

$$u_0 = -\sin x,$$

and the periodic boundary condition on $[0, 1]$. It has been proved in [20] that no solutions blow up for $\alpha \geq \frac{1}{2}$ and that some blow up for $\alpha < \frac{1}{2}$. Thus in this case $\alpha = \frac{1}{2}$ is a genuine boundary of regularity. See also [1, 6] for more recent works.

The equation is spatially discretized by the pseudo spectral method with 4096 grid points and temporally integrated by the fourth-order Runge-Kutta method with the

time step size 1.0×10^{-4}. The viscosity coefficient is set to $\nu = 0.1$. We apply the analyticity strip method to the energy spectrum is defined by

$$E(k,t) = \frac{1}{2} \sum_{k \le |k| \le k+1} |\tilde{u}(k)|^2,$$

where $\tilde{u}(k)$ is the Fourier transform of the velocity. We fit it in the following form

$$E(k,t) = Ak^{-n} \exp(-2\delta(t)k),$$

and monitor how $\delta(t)$ behaves in time. It is extremely difficult to resolve the values of $\delta(t)$ for $\alpha \approx \frac{1}{2}$ by the conventional least-squares fitting method with the double-precision arithmetic, since $\delta(t)$ tends to zero rapidly in finite time when α is near the critical value. Thus we estimate the values of A, n and $\delta(t)$ by assuming that the ansatz holds for the consecutive three wave numbers, i.e., k, $k+1$ and $k+2$. The value of $\delta(t)$ obtained by this pointwise fitting depends on the wavenumber k. However, as we have observed in the numerical computation of the vortex-sheet singularity formation[25], if the numerical solution is obtained very accurately, the value of $\delta(t)$ hardly depends on the wavenumber and can be determined accurately. Thus here the numerical integration of the Burgers equation was carried out with the 40-digits floating point arithmetic using a multiple precision arithmetic library, *Exflib*[18]. Thanks to this, we can resolve the value of $\delta(t)$ as accurately as $O(10^{-4})$.

We show in Fig.1 the time evolution of $\delta(2\pi t)$ for various values of α. (The factor 2π comes from the periodic boundary conditions in $[0,1]$.) There an exact relationship

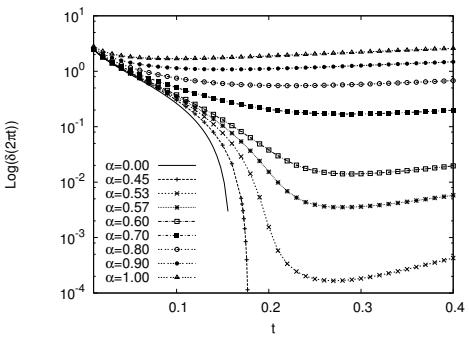

Figure 1. Time evolution of the analyticity strip $\delta(2\pi t)$ for the Burgers equation for various values of α.

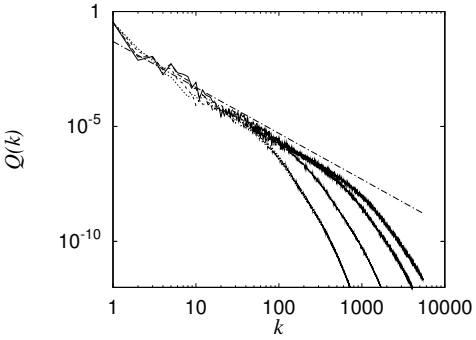

Figure 2. The spectra of active scalar for the inviscid case at $t = 7, 8, 9$ and 9.5 (from left to right). The straight line represents a slope -2.

for the inviscid case $\delta(t) = \log \frac{1+\sqrt{1-t^2}}{t} - \sqrt{1-t^2}$ [26] is also shown.

The numerical results show the following. If $\alpha > \frac{1}{2}$, $\delta(t)$ first decreases in time, but it starts to increase later, recovering the analyticity. On the other hand, if $\alpha < \frac{1}{2}$, it monotonically decreases in time and the velocity field becomes under-resolved quickly. By monitoring $\delta(t)$ we can distinguish regular and singular cases and confirm the result

[20], thereby gaining confidence with the analyticity strip method. We conclude that in this case the analyticity strip method does yield a useful guide regarding the regularity property of the solution.

3. Numerical results

We consider two kinds of initial data in this paper;

$$\text{Case 1} \quad \theta_0(\boldsymbol{x}) = \sin x \sin y + \cos y, \tag{1}$$

and

$$\text{Case 2} \quad \theta_0(\boldsymbol{x}) = \cos 2x \cos y + \sin x \sin y + \cos 2x \sin 3y. \tag{2}$$

They correspond to IC1 and IC3 in [9], respectively. We mainly treat Case 1 in detail and compare the results with those of Case 2 later.

First we consider the inviscid (ideal) case. As numerical methods we use a 2/3-dealiased Fourier pseudo-spectral method together with a four-stage Runge-Kutta method. Spatial resolutions used are typically 2048^2 and 4096^2 grid points for hypoviscous cases and up to 16382^2 for the ideal case. Temporal integration is performed with the fourth order Runge-Kutta method with the time step size typically, $\Delta t = 1 \times 10^{-3}$. All the computations have been done in double-precision arithmetic. Note that we do *not* implement the multiple precision arithmetic to the numerical computation of the SQG equations as in the case of the Burgers equation, for the reasons to be explained later. Some hypoviscous computations cover up to $t \leq 1000$. We mainly discuss the case of $\alpha = 0.4$, a supercritical case for which we have no proof of global regularity.

3.1. Initial condition 1

3.1.1. Long time evolution of the passive scalar We show in Fig.2 the inviscid evolution of the spectrum of the active scalar $Q(k)$, defined by

$$Q(k) = \frac{1}{2} \sum_{k \leq |\boldsymbol{k}| \leq k+1} |\tilde{\theta}(\boldsymbol{k})|^2,$$

where $\tilde{\theta}(\boldsymbol{k})$ is the Fourier transform of the active scalar. We confirm that the flow is well-resolved at $t = 7.0, 8.0, 9.0$ and 9.5. At $t = 10.0$ it is slightly under-resolved with a pile up at the highest wavenumber range (not shown).

In previous inviscid computations with 4096^2 modes, calculation were reliable up to $t \leq 7$. With a higher resolution of 16384^2 we may integrate the SQG equation a little bit far in time but in fact not too far, because the scaler gradient is increasing quite rapidly. In Fig.3 we show that thin layers of active scalar gradient formed in the domain.

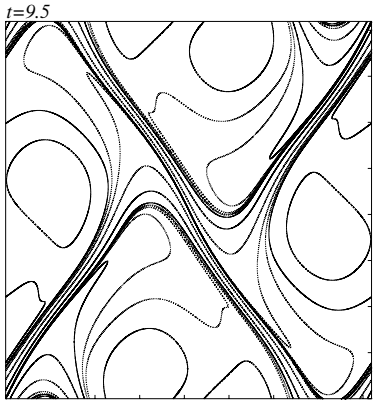

Figure 3. Contour plots of active scalar for the inviscid case at $t = 9.5$ in $[-\pi, \pi]^2$. Equally-spaced 10 thresholds are used between the maximum and minimum.

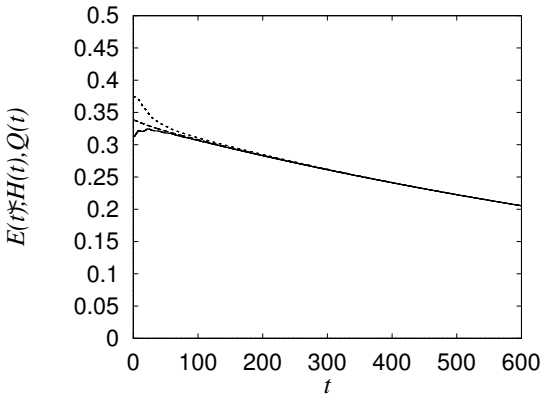

Figure 4. Time evolution of the several (squared) norms. The above figure shows $E(t)$ (solid) $H(t)$(dashed) and $Q(t)$(dotted) and the below one $P(t)$.

We begin discussing the hypoviscous computations, starting with the supercritical case of $\alpha = 0.4$. First we consider the time evolution of (squared) norms defined by

$$E(t) = \frac{1}{2}\sum_{\boldsymbol{k}} \frac{|\tilde{\theta}(\boldsymbol{k})|^2}{|\boldsymbol{k}|^2}, \quad H(t) = \frac{1}{2}\sum_{\boldsymbol{k}} \frac{|\tilde{\theta}(\boldsymbol{k})|^2}{|\boldsymbol{k}|},$$

$$Q(t) = \frac{1}{2}\sum_{\boldsymbol{k}} |\tilde{\theta}(\boldsymbol{k})|^2, \quad P(t) = \frac{1}{2}\sum_{\boldsymbol{k}} |\boldsymbol{k}|^2 |\tilde{\theta}(\boldsymbol{k})|^2.$$

The quantities $H(t)$ and $Q(t)$ are inviscid constants of motion. As we see in Fig.4 they decrease in time with a slight dissipative mechanism. It should be noted that $E(t), Q(t)$ and $H(t)$ almost collapse with each other for $t \geq 100$. This happens when essentially only one wavenumber mode is excited, as confirmed later. The norm of higher derivatives $P(t)$ increases rapidly in the early stage and later generally decreases in time (figure omitted). The norm $E(t)$, which is not an inviscid constant of motion, slightly increases in the initial stage and decays with time. Unfortunately, from these spatially global behaviours it is hard to understand the details of the property of the flow.

Before studying the spectra of active scalar by the analyticity strip method in detail, we give their time evolution in relatively early stage $t \leq 100$ in Fig.5. From this

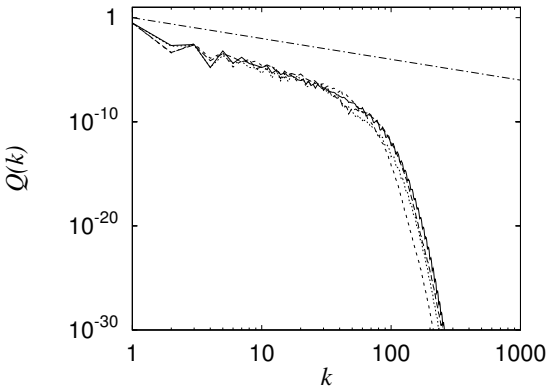

Figure 5. Time evolution of the spectra of active scalar at $t = 70$(solid), 80(dashed), 90(dotted), and 100(short-sashed). The straight line has a slope of -2.

we see that up to time of order $O(10^2)$ the spectra display a short power-law range, which has a slope steeper than that of the inviscid value -2, followed by an exponential fall-off. Again, by taking a look at this behaviour, we cannot understand the details of the analytic property.

After this time of order $O(10^2)$, we expect that the flow is on its way to eventual decaying process and it will converge to a trivial state of $\theta(\boldsymbol{x}) = 0$ in the end. In practice, it would take very long time for the flow to reach the final stage. To the authors's knowledge no detailed study has been reported on the behaviours in the very late stage.

We have conducted the direct numerical simulations for an unprecedentedly long time. In Fig.6 we show the time evolution of contours of active scalar up to $t = 50$. We observe that after the formation of a very thin layer of scalar gradient around $t = 10$, the flow pattern changes drastically by the effect of dissipativity. By $t = 50$, we see prominent structures parallel to the y-axis. In Fig.7 we show time evolution of contours of active scalar from $t = 100$ to 600. From $t = 100$ onward, the flow pattern is predominantly parallel to the y-axis. For example, at $t = 500$ and 600, the contours appear to be parallel to the y-axis almost perfectly. Recall if they were perfectly parallel the nonlinear term would vanish. Although the solution at the time $t = 600$ looks almost parallel at a glance, the width of $\delta(t)$ indicates that even at the time the nonlinear term does not identically vanish as we see later in Fig.25b below. An animations showing the time evolution of contours of active scalar is available online at `http://koji-ohkitani.staff.shef.ac.uk/papers.html`.

3.1.2. Oscillatory damping and the analyticity strip We then analyze the data by applying the analyticity strip method to the spectrum of the active scalar. We fit the

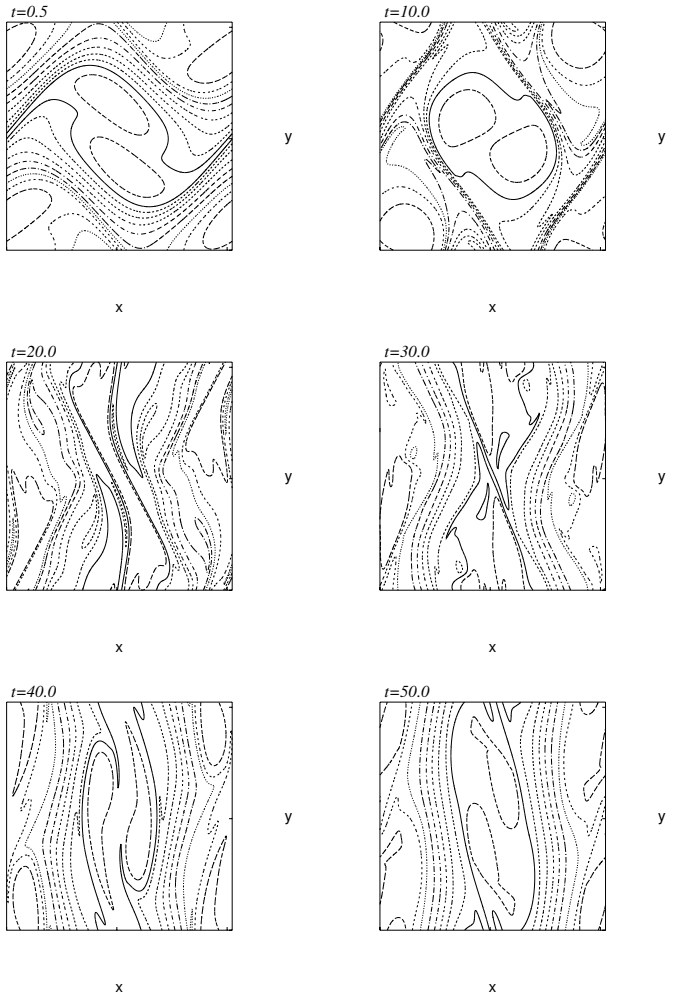

Figure 6. Contour plots of active scalar in $[0, 2\pi]^2$ at $t = 0.5, 10.0, 20.0, 30.0, 40.0$ and 50.0. Ten equally-spaced levels are used between the maximum and the minimum.

spectrum as

$$Q(k,t) = A(t)k^{-n(t)} \exp(-2\delta(t)k)$$

with three parameters $A(t), n(t)$ and $\delta(t)$ and watch how the width of the analyticity strip $\delta(t)$ recovers in time. (Time dependence of $Q(k,t)$ will be suppressed hereafter for simplicity.)

Unlike from the case of the Burgers equation, we apply the least-squares fitting. This is because the profile of the energy spectra for the solution of the SQG equation is oscillatory and is not as smooth as that for the Burgers equation even if the multiple precision arithmetic is implemented. For such oscillatory numerical data, the least-squares fitting gives more reliable estimate of $\delta(t)$ than the pointwise fitting. Moreover,

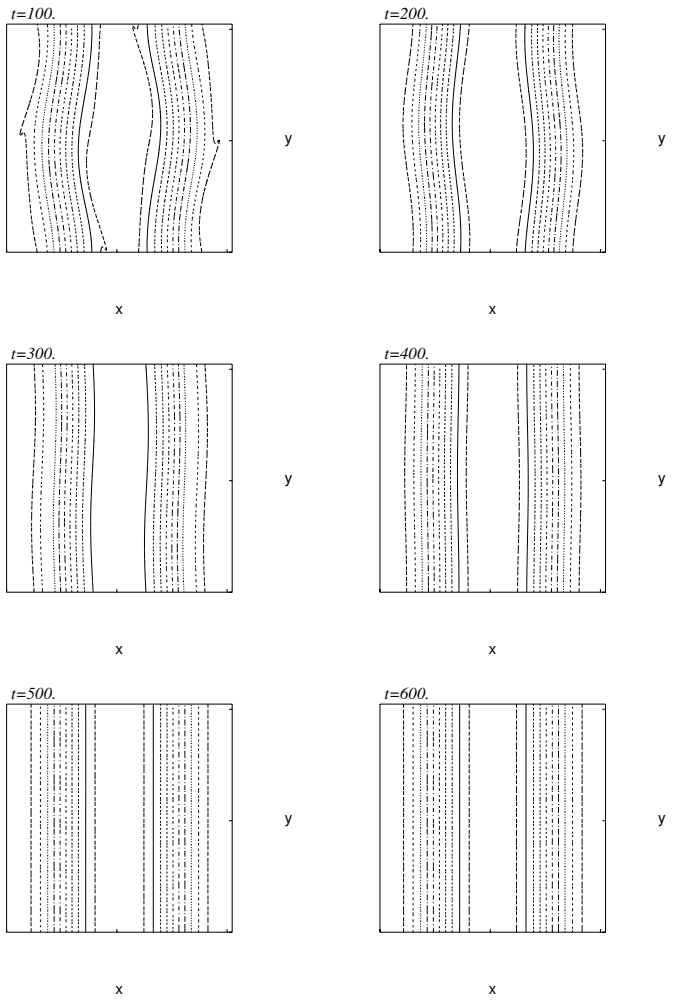

Figure 7. Contours of active scalar at $t = 100., 200., 300., 400., 500.$ and $600.$

we remove the lower-mode spectra up to the wavenumber $k = 15$ from the fitting data, since they suffer from violent oscillations. We have checked the level of the cut-off wavenumber is independent of the estimate of $\delta(t)$ as long as the high wavenumber components remain in the spectra.

In Fig.8 we show the time evolution of $\delta(t)$ up to $t = 300$. At the very early stage, the value of $\delta(t)$ drops very sharply, which is due to the formation of the sharp gradient of the scalars. The decrease of $\delta(t)$ soon stops due to the effect of the viscous dissipation, and then starts recovering the analyticity. After $t \geq 150$, we notice an unexpected behaviour in $\delta(t)$, that is, it oscillates around a certain level of analyticity. To examine the behaviour, we show in Fig.9 the time evolution of $\delta(t)$ up to $t = 600$. It is clear from this that the analyticity strip $\delta(t)$ is recovering its width in time *on*

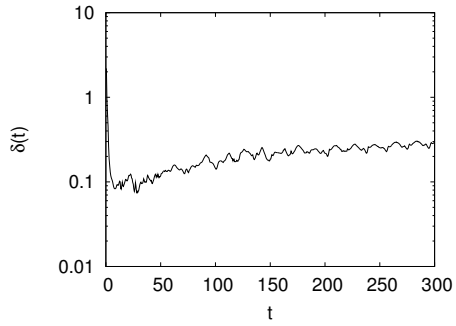

Figure 8. Time evolution of the analyticity strip $\delta(t)$ up to $t = 300$ for $\alpha = 0.4$ in a semi-log plot.

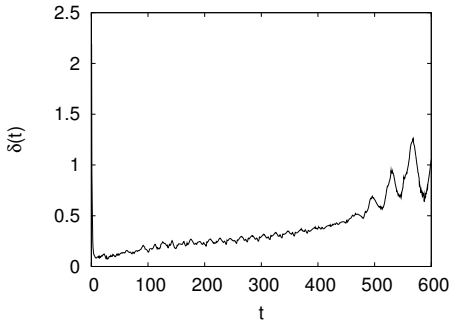

Figure 9. Time evolution of the analyticity strip $\delta(t)$ for $\alpha = 0.4$ up to $t = 600$.

average, but the oscillations observed in the previous Fig.8 persist to a later stage. For this initial condition with hypoviscosity, we have found an oscillatory damping process in the late stage of time evolution. A dip in $\delta(t)$ observed around $t = 600$ is actually an numerical artifact, which will be addressed later in subsection 3.1.3.

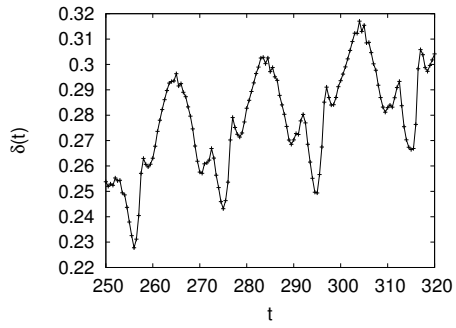

Figure 10. Time evolution of $\delta(t)$ for $\alpha = 0.4$ from $t = 250$ to 320 when the oscillatory damping is taking place.

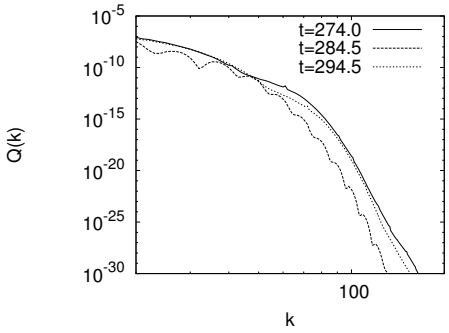

Figure 11. Snapshots of the spectra of the active scalar during one period of the oscillatory damping of $\delta(t)$ from $t = 274$ to $t = 294.5$.

We observe how the spectra of the scalars evolve when the oscillatory damping is taking place. Figure 10 shows the evolution of $\delta(t)$ between $t = 250$ and 320, in which we see three periods of the oscillation. We take one period from $t = 274.5$ to $t = 294.5$ and observe how the spectra of active scaler evolve in Fig.11. From $t = 274.$ to $t = 284.5$, the spectrum decreases due to the viscous dissipation, as a result of which $\delta(t)$ increases from the local minimum to the local maximum. Afterwards, the spectrum begins growing due to the nonlinear advection effect until $t = 294.5$ when $\delta(t)$ attains the local minimum again. Let us notice the following two facts. First, although the spectra at $t = 274.0$ are decaying smoothly, that at $t = 284.5$ where $\delta(t)$ attains local minimum after the viscous dissipation has a wavy profile. This means the viscous linear dissipation is prevented by the growth of spectra due to their nonlinear interactions. Second, after the one period of oscillation the distribution of the spectrum at $t = 294.5$

is lower than that at $t = 270.$, which means the solution gets a little bit smoother in the one period of oscillation. On the basis of this observation we infer that the oscillatory damping arises due to a subtle periodic balancing between the growth by the nonlinear advection and the damping by the linear viscous damping. Note also that the period ≈ 20 is on the same order of the large-scale turn-over time T, which may be estimated $T = 2\pi/\sqrt{3E/2} \approx 10$ using $E \approx 0.25$ at $t = 300$.

In order to understand this oscillatory damping in more detail, we compare the time evolution of analyticity strips for a number of different values of α in Fig.12. For all the values of α, still $\delta(t)$ recover in time with oscillations. If we use $\alpha = 0.3$, it does so a bit more slowly than the case of $\alpha = 0.4$ because of weaker dissipativity. On the other hand, for $\alpha > 0.4$, it grows rapidly than the case of $\alpha = 0.4$ Moreover, if we switch from $\alpha = 0.4$ (supercritical case) to $\alpha = 0.6$ (subcritical case) abruptly at $t = 300$, the analyticity starts to increase faster as in seen Fig.13, consistent with intuition.

A rather clear oscillatory behaviour suggests that there may be a periodic solution in the phase space for the ideal case. To check this possibility we switch off the dissipative term at $t = 300$ all of a sudden, to see if it converges toward an inviscid limit cycle that might possibly exist. However, as is clear from Fig.13, the analyticity strip rapidly decreases after switching to the inviscid evolution and the flow becomes under-resolved in a very short time. This shows that such an inviscid limit cycle does *not* exist. It also shows that in the stage of oscillatory damping with hypoviscosity, the nonlinear term and the linear dissipative term are in a subtle balance. We judge that the dynamics at that stage is *not* dominated by the dissipative term yet.

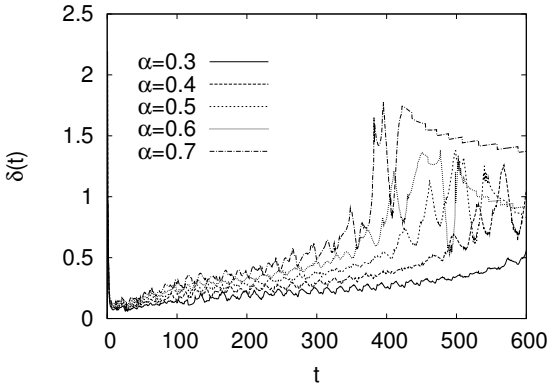

Figure 12. Time evolution of analyticity strip for different α.

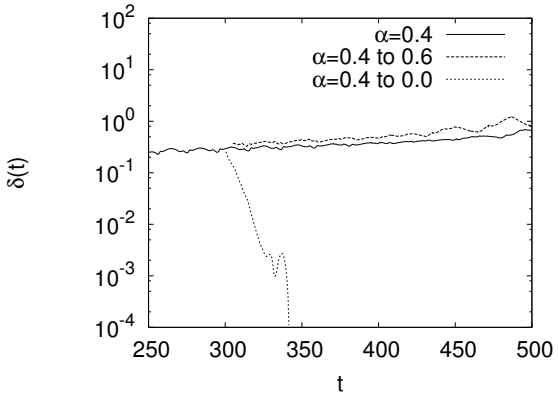

Figure 13. Time evolution of $\delta(t)$ for $\alpha = 0.4$(solid). The dashed line shows $\delta(t)$ after switching to $\alpha = 0$ at $t = 300$. Likewise, short-dashed line shows a switch to the inviscid case. Wavenumber modes with $k \leq 15$ have been removed for the fitting.

3.1.3. Analyticity strip and maximally excited mode In some of the cases we observe large fluctuations in the late stage, see again Fig.12. The larger values α takes, the sooner the wild fluctuations set in. It has turned out that the fluctuation comes from the fact that in the late stage of the evolution we have only limited number of modes that can be used for fitting $\delta(t)$. To confirm this view we introduce the concept of the maximally excited number, that is, the number k such that $Q(k) \geq 10^{-25}$. Time evolution of the maximally excited modes is shown in Fig.14 for various values of α. We find that once the maximally excited mode reaches about 60, the analyticity strip $\delta(t)$ starts to fluctuate violently.

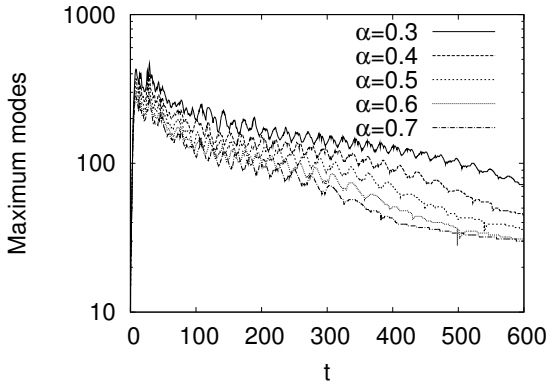

Figure 14. Time evolution of maximally excited number for different α.

The smaller α is, the longer the duration of oscillatory damping lasts. In order to understand this consistently with (expected) global regularity we examine the early stage behaviour in detail, by changing the values of ν. For the totally inviscid case, the analyticity strip $\delta(t)$ is observed to decrease exponentially in time. For the viscous case, if the viscosity is very small, the solution behaves nearly inviscidly, tracking the inviscid shrinkage of analyticity until the viscous effects become important. It should be noted that (i) by that time $\delta(t)$ is very small and (ii) it takes long to recover analyticity with prolonged oscillations because of small α.

The exponential decay of $\delta(t)$ for the inviscid case plays a vital role here, as it enables us to choose α and/or ν in such a way that recovery of $\delta(t)$ starts from an arbitrarily small value. If there *were* a finite-time blowup for the SQG equation, then we would have a fixed time, near which the viscous effects become important as we have observed in the case of the Burgers equation in Fig.1. If it were the case, all the above argument would have broken down.

In Fig.15 we plot the early time evolution of $\delta(t)$ for different values of ν, with α held fixed at 0.4. The smaller ν becomes (or, equivalently the larger the initial data are), the longer the viscous solutions track the inviscid evolution. This explains, at least partially, why it is difficult to prove regularity for $\alpha < \frac{1}{2}$.

In Fig.16 we plot the maximally excited modes. This shows that the number of excited modes also tracks that of the inviscid solution. Note that for $\nu = 0$ and $\nu = 2.5 \times 10^{-5}$, the graphs become flat after some time because of the cut-off at high wavenumber. All in all, the long-term oscillatory damping is entirely consistent with global regularity of the inviscid solution.

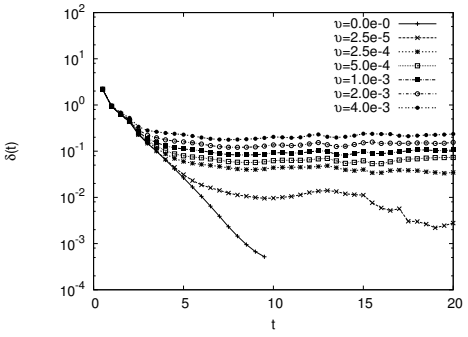

Figure 15. Time evolution of the analyticity strip with $\alpha = 0.4$ for several values of ν.

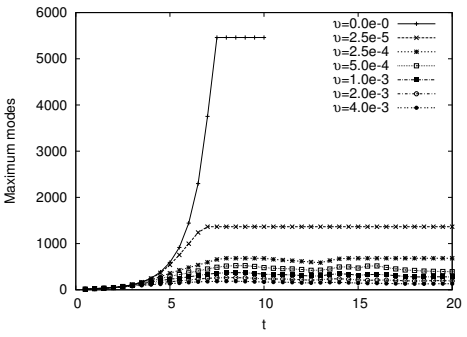

Figure 16. Time evolution of the the maximally excited modes with $\alpha = 0.4$ for several values of ν.

3.1.4. Very late stage Now, we examine the very late stage of the time evolution. In Fig.17 we show the over-all evolution of spectra for $\alpha = 0.4$. It shows how the excitation initially localised at low wavenumbers spreads over to the larger wavenumbers and then starts to decay. It should be noted that at $t = 300$ the spectrum begins to show oscillatory excitations in lower wavenumber range and this is even more pronounced at $t = 600$. In Fig.18 we show similar plots for $\alpha = 0.7$. Again, the spectrum shows oscillations at low wavenumbers. The physical mechanism of this oscillations is not known.

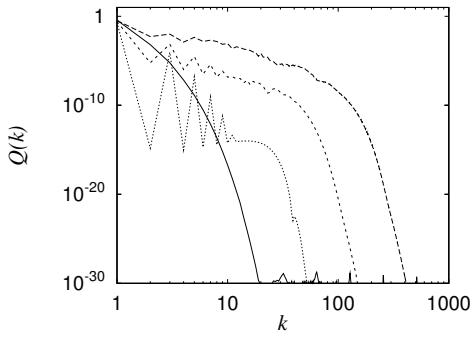

Figure 17. Spectra of active scalar at $t = .5$(solid), 10(dashed), 300(short-dashed) and 600(dotted) for $\alpha = 0.4$.

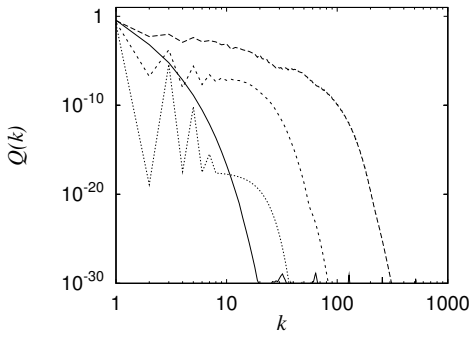

Figure 18. Spectra of active scalar at $t = .5$(solid), 10(dashed), 300(short-dashed) and 600(dotted) for $\alpha = 0.7$.

In order to examine the very late stage, where the numerical solution aligns the y

direction, it is useful to check 1D spectra defined by

$$Q(k_1) = \frac{1}{2}\sum_{k_2=0}^{\infty} |\tilde{\theta}(k_1, k_2)|^2,$$

and

$$Q(k_2) = \frac{1}{2}\sum_{k_1=0}^{\infty} |\tilde{\theta}(k_1, k_2)|^2.$$

In the Fourier transform

$$\tilde{\theta}(k_1, k_2) = \int_0^{2\pi}\int_0^{2\pi} \theta(x_1, x_2) e^{-i(k_1 x_1 + k_2 x_2)} \frac{dx_1 dx_2}{(2\pi)^2},$$

if we assume that the active scalar is independent of x_2, that is, $\theta(x_1, x_2) = \theta(x_1)$ we find

$$\tilde{\theta}(k_1, k_2) = \delta_{k_2,0} F(k_1),$$

where $\delta_{k_2,0}$ is Kronecker's delta and $F(k_1) = \int_0^{2\pi} \theta(x_1) e^{-ik_1 x_1} \frac{dx_1}{2\pi}$. Thus, if $\theta(\boldsymbol{x})$ is totally independent of x_2, $Q(k_2)$ has an excitation only at $k_2 = 0$. In this case we have

$$Q(k_1) = F(k_1) \text{ and } Q(k_2) = \delta_{k_2,0} \sum_{k_1=0}^{\infty} F(k_1).$$

In Fig.19 and 20 we show the over-all development of 1D spectra, which shows that $Q(k_2) \ll Q(k_1)$ at the late stage, if we compare at the same wavenumber $k_1 = k_2$. This is consistent with the observation that contours of $\theta(\boldsymbol{x})$ are almost parallel to y-axis. In

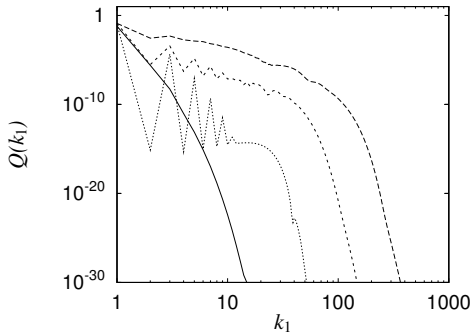

Figure 19. One-dimensional spectrum of active scalar $Q(k_1)$ for $\alpha = 0.4$ at $t = .5$, 10, 300, 600.

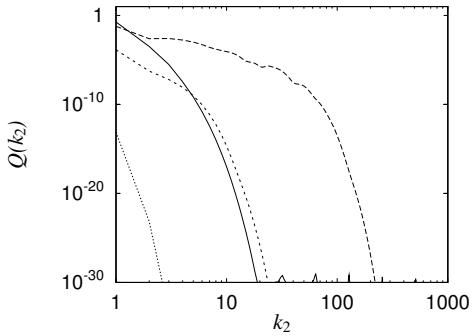

Figure 20. One-dimensional spectrum of active scalar $Q(k_2)$ for $\alpha = 0.4$ at $t = .5$, 10, 300, 600.

Fig.21 and 22 we show the late-stage development of 1D spectra, where a rapid decay of $Q(k_2)$ is seen. It is also seen that in $Q(k_1)$ the mode $k_1 = 1$ is decaying slowly is together with with odd-numbered modes $k_1 = 3, 5, \ldots$

In order to check if the higher harmonics survive or not we compute normalised spectrum defined by

$$\tilde{Q}(k) = \frac{Q(k)}{\sum_k Q(k)}.$$

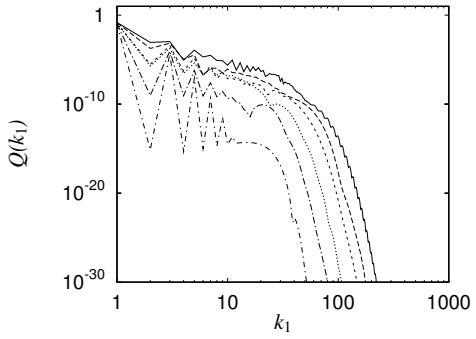

Figure 21. One-dimensional spectrum of active scalar $Q(k_1)$ for $\alpha = 0.4$ at $t = 100$, 200, 300, 400, 500, 600.

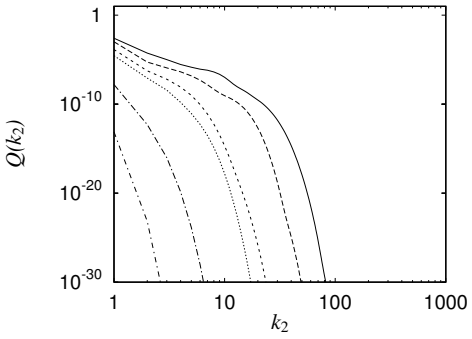

Figure 22. One-dimensional spectrum of active scalar $Q(k_2)$ for $\alpha = 0.4$ at $t = 100$, 200, 300, 400, 500, 600.

Note that if the excitation is strictly localised at $k = 1$ then $\tilde{Q}(k) = 1$ at $k = 1$, and $\tilde{Q}(k) = 0$ otherwise. In Fig.23, we show the phase portrait in $\tilde{Q}(1)$, $\tilde{Q}(3)$, which are the two largest excitations in the late stage. As time goes on, we see $\tilde{Q}(1) \to 1$, $\tilde{Q}(3) \to 0$, with the crowded symbols represent the late stage. In Fig.20 we plot a similar portrait for $\tilde{Q}(3)$, $\tilde{Q}(5)$, showing that both $\tilde{Q}(3)$ and $\tilde{Q}(5) \to 0$. We have also found similar results for $\alpha = 0.7$(figures omitted).

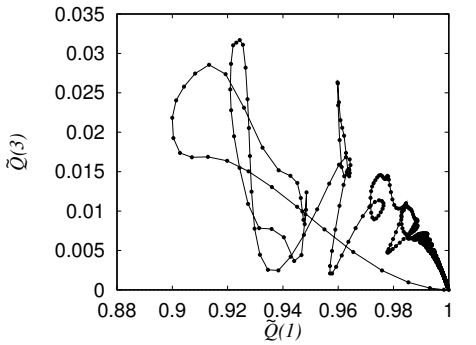

Figure 23. Phase portrait in normalised spectrum $\tilde{Q}(1) - \tilde{Q}(3)$ for $\alpha = 0.4$.

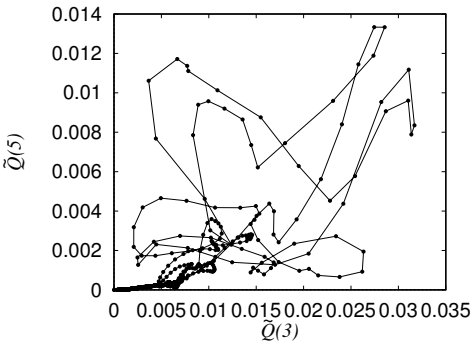

Figure 24. Phase portrait in normalised spectrum $\tilde{Q}(3) - \tilde{Q}(5)$ for $\alpha = 0.4$.

To take a closer look at the late stage behaviour compare the sub- and supercritical cases. We plot the time evolution of some of individual the Fourier coefficients of $|\boldsymbol{k}| = 1$ in Fig.25. We recall that the initial condition (1) reads in Fourier space

$$\tilde{\theta}(0, \pm 1) = \frac{1}{2}, \quad \tilde{\theta}(\pm 1, -1) = \pm\frac{1}{4}, \quad \tilde{\theta}(\pm 1, 1) = \mp\frac{1}{4}.$$

The coefficient $\mathrm{Re}(\tilde{\theta}(1, 0))$ sharply increases in the beginning and decays slowly subsequently. This is responsible for changing the contour pattern to the one with contours nearly parallel to the y-axis (Fig.25a). In Fig.25b we show a semi-logarithmic plot together with a linear decay rate: $\exp(-\nu t)$ (dashed line). The discrepancy is

noticeable, which confirms the nonlinear term is still effective. As for $\mathrm{Re}(\tilde{\theta}(0,1))$ which is responsible for $\sin y$, it sharply drops from its initial value $1/2$ and starts oscillating. The oscillation is visible up to $t = 400$ in the figure (Fig.25c). Figure 25d shows a phase portrait in these components; which shows $\tilde{\theta}(0,1)$ decays to 0 quickly whereas $\tilde{\theta}(1,0)$ does so very slowly. At $t = 600$, we have $\mathrm{Re}(\tilde{\theta}(1,0)) \approx 0.453$, which corresponds to $\theta(\boldsymbol{x}) \approx 0.9$, or to only 10 % decay from the initial value. A comparison has been made to the similar plots for $\alpha = 0.7$ (figures omitted), which shows a decay of $\tilde{\theta}(1,0)$ more rapid than for $\alpha = 0.4$ and which is closer to the linear decay rate $\exp(-\nu t)$.

In Fig.26 we plot the decay of $\tilde{\theta}(1,0)$, after compensating by $\exp(\nu t)$ for both α. It shows that even $\alpha = 0.7$ the decay is not a perfectly linear one but close to it. Noting $\mathrm{Re}(\tilde{\theta}(1,0)) \approx 0.378$ at $t = 600$, if we assume the linear decay rate for $t \geq 600$, the peak value of the active scaler is approximated as

$$\theta = 0.755 \exp(-\nu(t - 600)) \quad \text{with} \quad \nu = 0.001.$$

If we estimate how long it takes to have $|\theta| \leq \epsilon$, then we get $t > 600 + \frac{1}{\nu} \log \frac{0.755}{\epsilon}$. For example, in order for the active scalar to become as small as 1% of the initial value, we find $t > 4932$, which is much longer than the present coverage.

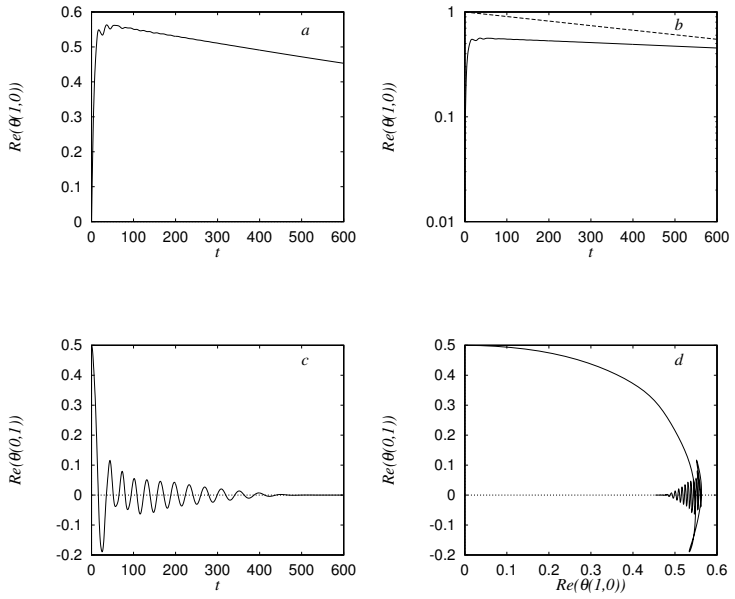

Figure 25. Time evolution of several Fourier coefficients for supercritical $\alpha = 0.4$, a: $\mathrm{Re}(\theta(1,0))$, b:its log-linear plot with a straight line $\exp(-\nu t)$, c: $\mathrm{Im}(\theta(1,0))$ and d: $\mathrm{Re}(\theta(0,1))$ vs. $\mathrm{Re}(\theta(1,0))$.

3.2. Initial Condition 2

Finally we briefly describe the other initial condition (2) of Case 2 with $\alpha = 0.4$ and with $\nu = 1 \times 10^{-3}$. In Fig.27 we show the time evolution of contour plots of the active scalar. The long time evolution is markedly different from Case 1 in that we have apparently

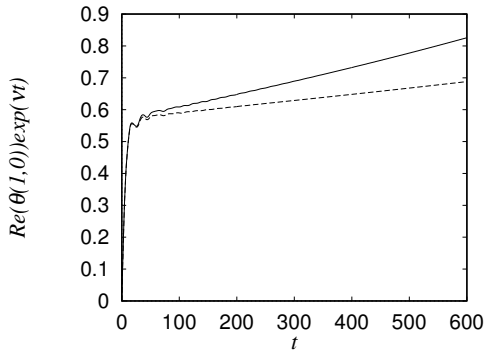

Figure 26. Time evolution of a Fourier coefficient compensated by $\exp(\nu t)$ for supercritical $\alpha = 0.4$ (solid) and subcritical $\alpha = 0.7$ (dashed).

regular arrays of vortices in the late stage rather than straight lines. However, even in this case the oscillatory damping does take place, and an oscillation is observed in the peripheral regions between the 'vortices'. Indeed, the time evolution of the analyticity strip shows in Fig.28 an oscillatory behaviour in the long run: $t \geq 400$. Also the figure shows the case when we switch suddenly to inviscid evolution at $t = 600$. As before $\delta(t)$ quickly decreases in time and the numerical solution gets under-resolved. This shows that the nonlinear and viscous terms are in a subtle balance in this case, too. Finally, we plot in Fig.29 the time evolution of the maximally excited number, which supports again the oscillatory behaviour in the late stage of the time evolution.

All in all, this result suggests that the long-term oscillatory damping found here is not restricted to Case 1 but rather it is a phenomenon common to many initial data.

4. Summary and discussion

In an attempt to shed some light upon the regularity problems of the SQG equations actively discussed recently, we have numerically investigated their analytic property in the long-term evolution. We have found an oscillatory damping in the late stage with a subtle balance between nonlinear and dissipative terms. This suggests that it may be a serious obstacle that cutting-edge mathematical analysis is facing.

Inviscid solutions are also treated numerically. The analyticity strip decreases exponentially in time and it takes arbitrarily small values as time proceeds and they do not appear to blow up in finite time. For slightly viscous cases, we can construct solutions as close as the inviscid one, independent of α. However, by the effect of α, sooner or later the viscous solution deviates from the inviscid one, relaxing toward smoother solutions.

As far as the present computations are concerned, the relaxation process is closer to a linear damping process for the subcritical case $\alpha > 1/2$, but a nonlinear damping

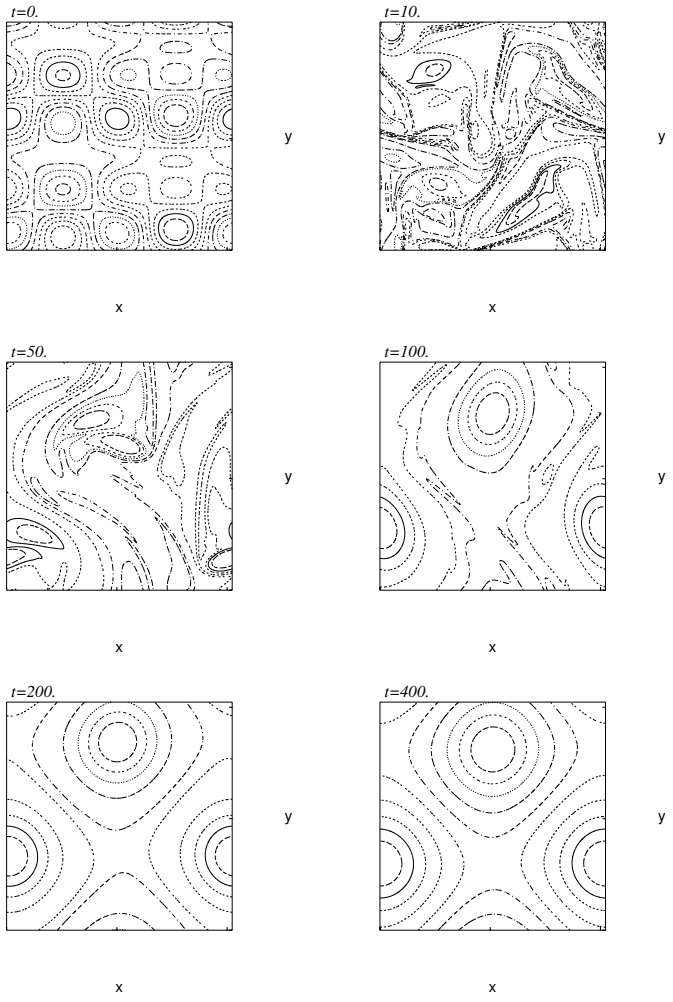

Figure 27. Contours of active scalar for the initial data (2) at $t = 0.$, 5.0, 10.0, 100.0, 200.0 and 400.0, plotted as in Fig.6.

for the supercritical case $\alpha < 1/2$. For fixed ν, the smaller α is the longer time it takes for recovering the analyticity. However, it should be noted that no sharp qualitative change around $\alpha = 1/2$ has been observed in the numerical results, suggesting that the boundary $\alpha = 1/2$ is of artificial and technical nature.

Taking smaller ν (or, larger initial norms) the analyticity deteriorates as bad as the inviscid solution and the relaxation thereafter takes place extremely slowly. To make progress in mathematical analysis, it may be necessary to consider nonlinear relaxation and relaxation time.

There exist mathematical frameworks in which one attempts to connect large-time asymptotics of the Navier-Stokes equations with eigenfunctions of Stokes operators

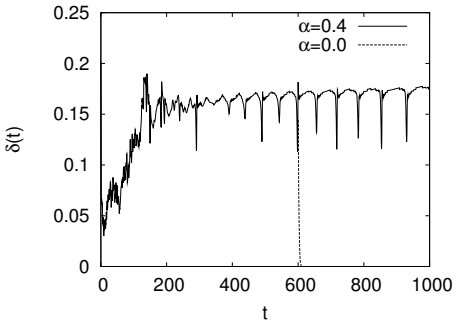

Figure 28. Time evolution of the analyticity strip $\delta(t)$ up to $t = 1000$. for Case 2 with $\alpha = 0.4$.

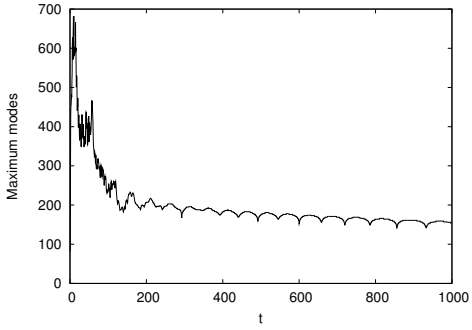

Figure 29. Time evolution of maximally excited number up to $t = 1000$. for Case 2 with $\alpha = 0.4$.

assuming global regularity. One such framework is called normal form theory [13, 14, 16, 15]. Assuming that a similar framework works for the SQG equations (we are not aware of articles on such frameworks for the SQG equation), we may write

$$\theta(t) \sim \sum_{n=1}^{\infty} W_n(\theta_0, t) \exp(-\nu n t),$$

as large-time asymptotics. By normal form, we mean a map from $\theta(0)$ to $(W_n(0))_{n=1}^{\infty}$. The polynomials $W_n(\theta_0, t)$ could in principle be computed recursively from the normalisation map $W(\theta_0)$ by the nonlinear terms of the SQG equation. Constructing $W_n(t)$ specifically and comparing it with the numerics will be an interesting direction to pursue.

Acknowledgments

This work has been partially supported by an EPSRC grant EP/F009267/1. Koji Ohkitani has been supported by Royal Society Wolfson Research Merit Award. Part of this work has been presented at a workshop "The 3D Euler and 2D surface quasi-geostrophic equations" (March 30 to April 10, 2009) at American Institute of Mathematics, and also at a SIAM Conference on "Analysis of Partial Differential Equations" (December 7 to 10, 2009) in Florida. Takashi Sakajo is partially supported by JSPS grant 21340017 and by JST PRESTO Award. We thank P. Constantin for discussion.

References

[1] Alibaud N, Imbert C and Karch G 2010 Asymptotic Properties of Entropy Solutions to Fractal Burgers Equation *SIAM J. Math. Anal.* **42** 354–376

[2] Bardos C, Penel P, Frisch U and Sulem PL 1979 Modified dissipativity for a non-linear evolution equation arising in turbulence *Arch. Rat. Mech. Anal.* **71** 237–256

[3] Constantin P, Nie Q and Schörghofer 1998 Nonsingular surface quasi-geostrophic flow *Physics Letters A* **241** 168–172

[4] Caffarelli L and Vasseur A Drift diffusion equations with fractional diffusion and the quasi-geostrophic equation, to appear.
[5] Chae D 2006 On the Regularity Conditions for the Dissipative Quasi-geostrophic Equations *SIAM J. Math. Anal.* **37** 1649–1656
[6] Chan CH, Czubak M and Silvestre L 2010 Eventual regularization of the slightly supercritical fractional Burgers equation *Disc. Cont. Dyn. Sys.* **27** 847–861
[7] Constantin P 2008 Singular, weak and absent: Solutions of the Euler equations *Phys. D* **237** 1926–1931
[8] Constantin P and Wu J 2008 Regularity of Hölder continuous solutions of the supercritical quasi-geostrophic equation *Ann. Inst. Henri Poincaré, Anal. Non Linéaire* **25** 1103–1110
[9] Constantin P, Majda A J and Tabak E 1994 Formation of strong fronts in the 2-D quasigeostrophic thermal active scalar *Nonlinearity* **7** 1495–1533
[10] Constantin P, Majda A J and Tabak E 1994 Singular front formation in a model for quasigeostrophic flow *Phys of Fluids* **6** 9–11
[11] Cordoba A and Cordoba D 2004 A maximum principle applied to quasi-geostrophic equations *Commun. Math. Phys.* **249** 511–528
[12] Deng J, Hou TY, Li R and Yu X 2006 Level Set Dynamics and the Non-blowup of the 2D Quasi-geostrophic Equation *Methods Appl. Anal.***13** 157–180
[13] Foias C, Hoang L, Olson E and Ziane M 2006 On the solutions to the normal form of the Navier-Stokes equations *Indiana University Mathematics Journal* **55** 631–686
[14] Foias C, Hoang L, Olson E and Ziane M 2009 The normal form of the Navier-Stokes equations in suitable normed spaces *Ann. Inst. Henri Poincaré, Anal. Non Linéaire* **26** 1635–1673
[15] Foias C and Saut JC 1987 Linearization and normal form of the Navier-Stokes equations with potential forces *Ann. Inst. Henri Poincaré, Anal. Non Linéaire* **4** 1–47
[16] Foias C and Saut JC 1982 Transformation fonctionnelle linéarisant les equation de Navier-Stokes *CR Acad. Sci. Paris, Série I, Math.* **23** 325–327
[17] Friedlander S, Pavlovic N and Vicol V 2009 Nonlinear Instability for the Critically Dissipative Quasi-Geostrophic Equation *Commun. Math. Phys.***292** 797–810 (2009)
[18] Fujiwara H, Extend precision floating-point arithmetic library(Exflib) is available at `http://www-an.acs.i.kyoto-u.ac.jp/~fujiwara/exflib/index.html`
[19] Kiselev A, Nazarov F and Volberg A 2006 Global well-posedness for the critical 2D dissipative quasi-geostrophic equation *Invent. math.* **167** 445–453
[20] Kiselev A, Nazarov F and Shterenberg R 2008 Blow Up and Regularity for Fractal Burgers Equation *Dyn. Partial Differ. Equ.* **5** 211–240
[21] Majda A J and Tabak E G 1996 A two-dimensional model for quasigeostrophic flow: comparison with the two-dimensional Euler flow *Physica D* **98** 515–522
[22] Niche CJ and Schonbek ME 2007 Decay of Weak Solutions to the 2D Dissipative Quasi-Geostrophic Equation *Commun. Math. Phys.* **276** 93–115
[23] Ohkitani K and Yamada M 1997 Inviscid and inviscid-limit behavior of a surface quasi-geostrophic flow *Phys. Fluids* **9** 876–882
[24] Silvestre L 2010 Eventual regularization for the slightly supercritical quasi-geostrophic equation *Ann. Inst. Henri Poincaré, Anal. Non Linéaire* **27** 693–704
[25] Shelley M J 1992 A study of singularity formation in vortex-sheet motion by a spectrally accurate vortex method it J. Fluid Mech. **244** 493–526
[26] Sulem C, Sulem PL and Frisch H 1983 Tracing complex singularities with spectral methods *J. Comput. Phys.* **50** 138–161
[27] Wu J 2005 Global Solutions of the 2D Dissipative Quasi-Geostrophic Equation in Besov Spaces *SIAM J. Math. Anal.***36** 1014–1030